Journal of Applied Polymer Science

Morphological Analysis of Crease Patterns Formed on Surface-Attached Hydrogel with a Gradient in Thickness

Jungwook Kim
Department of Chemical and Biomolecular Engineering, Sogang University, Seoul 121-742, Republic of Korea
Correspondence to: J. Kim (E-mail: jungwkim@sogang.ac.kr)

ABSTRACT: The morphology of crease pattern formed on the surface-attached hydrogel with a gradient in thickness is analyzed. We label the hydrogel surface at the creased state with fluorescent polyelectrolyte, which enables us to visualize surface morphology of creases using the fluorescent microscopy. Various morphological features of crease patterns are analyzed at different thickness of hydrogel, or characteristic spacing of creases $\lambda_{c,\max}$, to examine the self-similarity of crease morphology at different length scales. Some morphological features show no $\lambda_{c,\max}$ dependence, implying the self-similarity, while others show weak $\lambda_{c,\max}$ dependence with positive values of the exponent of power law fit for the plots. We infer that such nonself-similarity is originated from the variations in the kinetics of swelling and creasing of hydrogel, the effect of surface tension, or the reduction in the osmotic pressure occurred during the polyelectrolyte labeling step at different $\lambda_{c,\max}$. © 2014 Wiley Periodicals, Inc. J. Appl. Polym. Sci. **2014**, *131*, 40482.

KEYWORDS: gels; swelling; stimuli-sensitive polymers; crosslinking; morphology

Received 29 October 2013; accepted 20 January 2014
DOI: 10.1002/app.40482

INTRODUCTION

Formation of periodic microstructures on the surface of elastic materials by instabilities, for examples, creasing of surface-attached hydrogel films or wrinkling of surface-modified PDMS films, has been of interests in the last decade. During the period, researchers began to consider such instabilities not merely as defects or failures that should be avoided during manufactural processes, but as the fundamental topic in mechanics that can further be utilized in a number of technologies.[1–5] For examples, researchers have harnessed the instabilities to fabricate micro-structures with tunable properties[6–12] or measure mechanical properties of thin films that otherwise would be hard to quantify.[13–15] Particularly, the elastic creasing instability of surface-attached hydrogel has been utilized to fabricate dynamic surface patterns,[8,11] guide stem cell adhesion,[16] or explain morphological evolution of organs.[17] In general, the creasing instability occurs when the swelling of hydrogel film is mechanically constrained by the underlying rigid substrate and thereby generated inplane compression exceeds the critical value for the instability.

Creases formed on the surface-attached hydrogel can be quantified in terms of its morphological features. One representative morphological feature of creases is their characteristic length scale, i.e., the average lateral distance between creases. Unless surface-attached hydrogels contain inhomogeneity, for example, topographic patterns on underlying substrates[8,11] or defects on hydrogel surface,[18] whose length scales affect those of growing creases, or unless lateral sizes of hydrogel are similar to or less than the thickness of hydrogel, the thickness of hydrogel should be the only length scale associated with the crease formation. Furthermore, if material properties such as Young's modulus and equilibrium swelling ratio, which is defined by the fractional increase in the volume of hydrogel due to water absorption of as-prepared hydrogel, are identical, the thickness of hydrogel is the only variable determining the characteristic length scale of creases. Experimentally, the characteristic length scale of creases is found to be almost linearly proportional to the thickness of hydrogel.[2] The theoretical model based on the linear perturbation analysis predicts a power-law relationship between the characteristic length scale of creases and the thickness of hydrogel with the power-law exponent of ~0.9 over the gel thickness.[19]

Although a number of previous studies investigated the dependence of the characteristic length scale of creases on the thickness of hydrogel, there are still a number of other morphological features that need to be analyzed quantitatively to better understand the formation of crease; for examples, the evolution of crease morphology, i.e., two-dimensionally periodic structure with the characteristic length scale, or the effect of swelling kinetics on the morphological evolution. Specifically, we investigate two-dimensional connectivity, depth, or curviness of creases, polygonal arrangement of creases, or distribution of

crease lengths at different thickness of hydrogel. Such thickness-dependent analysis enables us to determine the morphological self-similarity of crease patterns at different length scales along both inplane and out-of-plane directions. We use the hydrogel with a gradient in thickness such that the morphological features can be compared at various thicknesses by a single system. The use of the single system is important as, beside its efficiency, even slight sample-to-sample variations in either the preparation of hydrogels, e.g., degree of polymerization, or the experimental condition, e.g., a temperature of water immersion bath, could significantly alter the crease morphology. To better quantify the shape of creases, we coat surface areas of hydrogel, except the regions folded within creases, with fluorescently labeled polymer. This method provides contrast in fluorescent intensity between creased (folded) and remaining (not folded) areas of hydrogel surface, and therefore, allows us to estimate the shape of creases along both inplane and out-of-plane directions. We expect that the analytical method used in the current study to quantify the morphological features of creases could be applied as well to analysis of other periodic microstructures formed on the surface of thin film, e.g., crack, wrinkle, or fold.

EXPERIMENTAL

Synthesis of Surface-Attached Hydrogel with a Gradient in Thickness

To enable a covalent attachment of hydrogel on the glass coverslip, which mechanically confines the swelling of hydrogel, the surface of the coverslip was functionalized with methacrylate group. Briefly, the glass coverslip was activated with an oxygen plasma for 10 min and immersed in ethanol containing 0.4 vol % of 3-(trichlorosilyl)propyl methacrylate for 8 h. The glass capillary channel with a gradient in channel thickness was assembled from the silanized coverslip, a bare coverslip, and a spacer that determines the channel thickness at one side. The capillary channel was loaded with a 1 mL of aqueous pregel solution containing 857 m*M* of *N*-isopropylacrylamide (NIPAM), 18 m*M* of sodium acrylate (NaAc), 9 m*M* of *N,N′*-methylenebisacrylamide (BisAAm), 1.5 μL of *N,N,N′,N′*-tetramethylethylenediamine and 5.0 μL of 10 wt % aqueous ammonium persulphate solution. Polymerization was allowed to proceed under nitrogen environment for 30 min, and thereby formed hydrogel was immersed in water for several hours to diffuse unreacted monomers out of the hydrogel and reach the equilibrium swelling. Although silane groups attached on the coverslip are hydrophobic, their effect on the swelling of hydrogel is negligible due to a large difference in the length scale between hydrophobic effect (less than a few nanometers) and the thickness of hydrogel (on the order of 10^1-10^2 μm). All the reagents were purchased from Sigma-Aldrich and used as-received.

Deposition of Fluorescent Polyelectrolyte on Surface of Hydrogel at Creased State

To visualize the shape of creases formed on the surface-attached hydrogel, the hydrogel at creased state was immersed in 1 mg/mL aqueous solution of fluorescently labeled poly(L-lysine) (PLL-FITC) (10 m*M* phosphate buffered saline, pH 7.0) for 3 s, followed by a rapid and thorough washing of the hydrogel surface with DI water. PLL-FITC was synthesized by dissolving 10 mg of PLL ($M_w = 150 - 300$ kg/mol) and 0.57 mg of FITC (fluorescein isothiocyanate) in 3 mL of DMSO (dimethyl sulfoxide) containing 40 μL of TEA (triethylamine), and the reaction proceeded for 10 h. The product was dialyzed (10 kDa molecular weight cutoff, Spectra/Por) against 10 m*M* PBS (phosphate buffered saline, pH 7.0) for 1 day and DI water for 2 days and finally lyophilized to yield PLL-FITC. A neutral pH (7.0) and low ionic strength (10 m*M* PBS) aqueous solvent was used in the deposition of PLL-FITC to promote electrostatic interaction between the positively charged PLL and the negatively charge poly(NIPAM-*co*-NaAc) hydrogel. Such solvent selection also increases the hydrodynamic radius of PLL, which retards diffusion of PLL into hydrogel, and therefore, restricts the adsorption of PLL only within the shallow depth from the hydrogel surface. All the reagents were purchased from Sigma-Aldrich and used as-received.

Fluorescent Imaging of Hydrogel Surface

An inverted optical microscope (Zeiss Axio Observer, 10× objective) equipped with a fluorescence excitation light source and a microscope stage heater was used to image hydrogel surface. Hydrogel whose surface was deposited with PLL-FITC at creased state was immersed in a water bath maintained at 37°C, which reduces the swelling ratio of hydrogel below the critical point of creasing. Fluorescent patterns on the surface of hydrogel at deswelled state were imaged at different lateral positions, which correspond to average thickness of 20, 25, 35, 45, 55, 65, 80, 100, and 120 μm for the hydrogel at the as-prepared state.

Morphological Analysis of Crease Patterns

ImageJ (National Institutes of Health, USA) was used to analyze morphology of crease patterns. Prior to the images analysis, background intensity was subtracted to account for uneven illumination across the entire field of view. A 2D Fourier transformation was performed on the fluorescent micrographs using Fast Fourier Transform (FFT) method, from which the frequency at the maximum FFT intensity was obtained. The obtained frequency was then inverted to calculate the characteristic length scale of creases $\lambda_{c,\max}$ at each gel thickness. The gray scale fluorescent micrographs of crease patterns were also converted to binary images to obtain skeletonized profiles of crease patterns, from which various morphological features of creases were analyzed using the ImageJ plugin 'AnalyzeSkeleton'.

RESULTS AND DISCUSSION

Formation of Creases on a Hydrogel with a Gradient in Thickness

We fabricate the surface-attached hydrogel with a gradient in thickness by assembling the asymmetric glass capillary channel (Figure 1). The asymmetric channel consists of the coverslip functionalized with methacrylate groups to covalently attach hydrogel to the coverslip, the un-functionalized coverslip to be released after hydrogel formation, the 170 μm thick glass spacer placed on one side of the channel, and two clamps that hold the assembly at each side of the channel [Figure 1(a)]. The aqueous pregel solution containing temperature-responsive NIPAM, anionically charged NaAc, cross-linker BisAAm as well as APS and TEMED that respectively initiates and catalyzes the

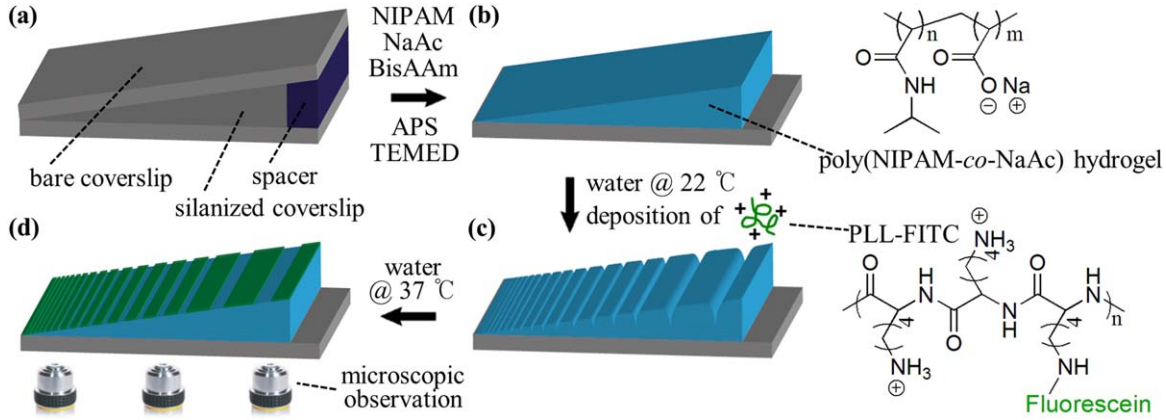

Figure 1. Fabrication of the surface-attached hydrogel with a gradient in thickness. (a) The glass capillary channel assembled from the silanized coverslip, a bare coverslip, and a spacer. (b) Formation of hydrogel through a radical polymerization of NIPAM, NaAc, and BisAAm within the capillary channel. (c) Deposition of fluorescent polyelectrolyte, PLL-FITC, on the surface of hydrogel through the formation of polyelectrolyte complex to visualize the shape of creases. (d) Microscopic observation of the surface of hydrogel at the deswelled state (37°C). [Color figure can be viewed in the online issue, which is available at wileyonlinelibrary.com.]

polymerization is loaded into the capillary channel, and the formation of hydrogel is proceed for 30 min [Figure 1(b)]. Upon detaching the un-functionalized coverslip and immersing the hydrogel attached to the functionalized coverslip into DI water, the hydrogel swells and forms creases on the surface, where the characteristic length scale of creases varies with the local thickness of hydrogel [Figure 1(c)]. The hydrogel at the creased state is immersed in the aqueous solution of fluorescently labeled polyelectrolytes, PLL-FITC, which diffuse into hydrogel and adsorb to oppositely charged polymeric backbone of hydrogel through the electrostatic interaction. However, diffusion and adsorption of PLL-FITC in the vicinity of creases are suppressed as highly compressed polymeric networks near self-contacted creases act as barriers for the diffusion of polyelectrolytes.[8] Therefore, the surface areas folded within creases are excluded from the polyelectrolyte deposition. Increasing the temperature of water immersion bath to 37°C reduces the swelling ratio of NIPAM-based hydrogel below the critical point of crease formation. Therefore, creases unfold, and the surface areas priorly folded within creases, thus not deposited by PLL-FITC, are exposed on the hydrogel surface, which provides contrast in fluorescent intensity between creased (folded) and remaining (not folded) areas of hydrogel surface [Figure 1(d)]. The surface of hydrogel at deswelled state is then imaged using the fluorescent microscope at several different positions along the direction of varying hydrogel thickness. Here, we use NIPAM as the major component of hydrogel such that increasing temperature of water immersion bath becomes a stimulus for triggering unfolding, and therefore, visualization of creases. Use of other common stimuli, for example, a change in pH or salinity of water immersion bath or irradiation of light, to trigger unfolding of creases is disadvantageous as such stimuli could either lead to desorption or photo-bleaching of deposited PLL-FITC, respectively.

Fluorescent micrographs of the surface of hydrogel at different lateral positions, thus with varying thickness, are shown in Figure 2(a), which reveal the regions of hydrogel surface once folded within creases. It is clearly shown that the characteristic size of fluorescent patterns, which reflects the characteristic length scale of creases, decreases with the thickness of hydrogel as reported in the previous studies. We perform 2D Fourier transform on fluorescent micrographs taken at nine different

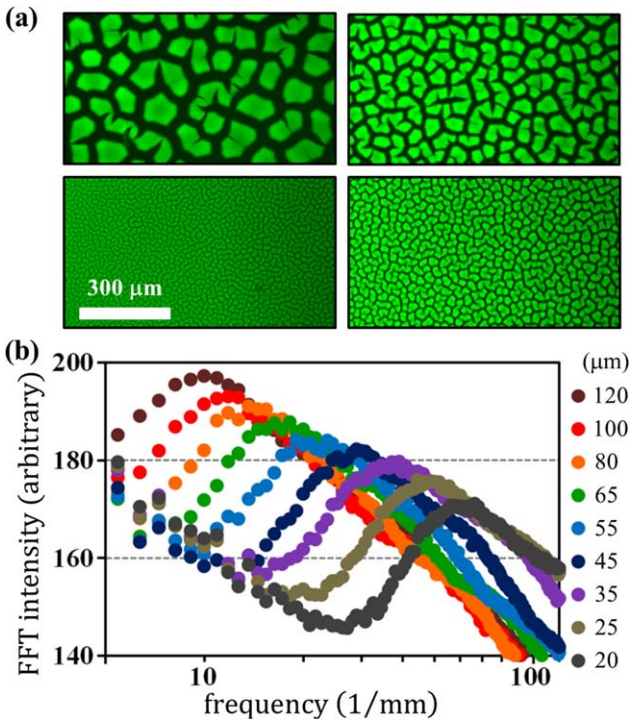

Figure 2. Formation of creases on the surface of hydrogel at varying thickness. (a) Fluorescent micrographs of the surface of hydrogel at 37°C, which reveal the area of surface once folded within creases (black-colored). Thicknesses of hydrogels at the as-prepared state are 120, 65, 35, and 20 μm (clockwise from the upper-left image). (b) A plot of FFT intensity of the fluorescent pattern on the surface of hydrogel against frequency, from which $\lambda_{c,max}$ is determined at varying thickness. [Color figure can be viewed in the online issue, which is available at wileyonlinelibrary.com.]

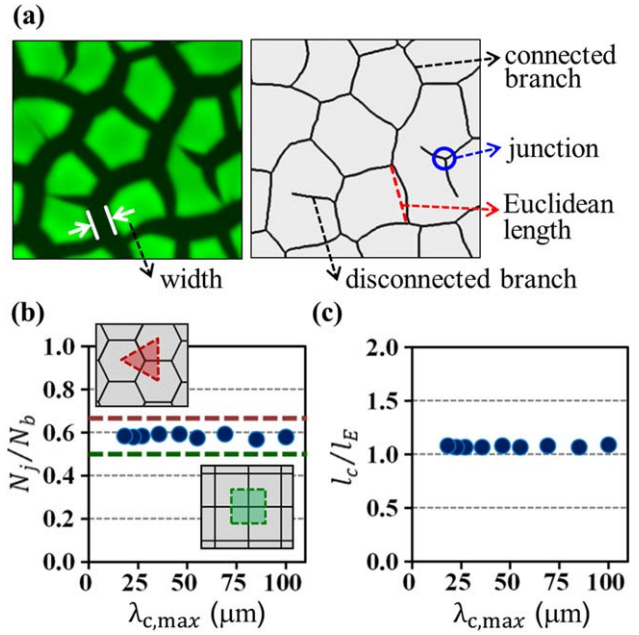

Figure 3. Morphological self-similarity of creases formed on the surface of hydrogel with a gradient in thickness. (a) A linear profile of creases (right), which indicates the inplane location of surface folding, obtained by skeletonizing the fluorescent micrograph (left). (b) A plot of the average value of N_j/N_b against $\lambda_{c,max}$. A red and a green dashed line represent the value of N_j/N_b for the ideal HCP and the square lattice structure, each of which is illustrated in an upper and a lower inset, respectively. A red triangle and a green square in the insets indicate the single unit cell of the HCP and the square lattice structure, respectively, from which the values of N_j/N_b are calculated. (c) A plot of the average value of l_c/l_E, an indicative of the curviness of creases, against $\lambda_{c,max}$, where almost constant value of 1.08 is obtained for l_c/l_E regardless of $\lambda_{c,max}$. The exponents of power law fits for the plots in (b) and (c) are on the order of 10^{-3}. [Color figure can be viewed in the online issue, which is available at wileyonlinelibrary.com.]

positions on the hydrogel surface [Figure 2(b)], and find that there is almost linear correlation between the thickness of hydrogel and the characteristic length scale of creases $\lambda_{c,max}$ with the exponent of power law fit of 0.98, which is close to the previously reported values.[2,19]

Morphological Self-Similarity of Crease Patterns Formed on the Hydrogel with a Gradient in Thickness

For a quantitative analysis of morphological features of crease patterns, dimmed areas in fluorescent micrographs, which indicate the regions of hydrogel surface folded within creases, are skeletonized [Figure 3(a)]. The resultant linear profiles, which are centerlines equidistant from boundaries of dimmed areas, are indicative of the locations of creases formed on swollen hydrogel. As illustrated in Figure 3(a), we define a number of basic geometric units for a systematic analysis of crease patterns, which include branch (connected or disconnected)—singe undivided line of crease, junction—a point at which three branches meet, Euclidean (or contour) length—a shortest (or the maximum end-to-end) distance of a branch, and width of crease—a distance perpendicular to the skeletonized centerlines and between boundaries of dimmed areas. Based on the basic geometric units, we analyze a number of morphological features of crease patterns and their self-similar characters by comparing them at various $\lambda_{c,max}$. Here, we set $\lambda_{c,max}$, instead of the hydrogel thickness, as the variable for comparing the morphological features of creases because $\lambda_{c,max}$ is more fundamental length scale in analyzing crease morphology than the thickness of hydrogel.

First, we measure the ratio of the number of junction to that of branch, N_j/N_b, to predict how densely creases are packed at each $\lambda_{c,max}$ [Figure 3(b)]. Creases form on the surface of hydrogel to release inplane equi-biaxial compressive stress by locally folding the surface of hydrogel. Therefore, it is desired that the surface area of folding is maximized, so is the packing density of creases, such that the hydrogel experiences the minimum amount of compressive stress. Achieving the maximum packing density of creases is analogous to that of equi-radial elastic circles expanding in 2D space. Initial swelling of hydrogel at every point on the surface is anisotropic and symmetric along the inplane direction, which, therefore, can be represented as equi-radial circles expanding at the same rate. In addition, nucleation of creases can be represented as the formation of nonconforming contact between circles that expanded large enough to fill almost entire space, and further growth of creases can be considered as the formation of nonadhesive and elastic contact lines between adjoining deformed circles. For an ideal case, equi-radial circles expanding in 2D space rearrange themselves into the hexagonal close packing (HCP) structure, which has the maximum packing density. Similarly, if creases form in the HCP structure, a single unit cell contains one junction and 3/2 branches as shown in Figure 3(b) (an upper left inset), thus the value of N_j/N_b becomes 2/3. If creases form in the square lattice structure [Figure 3(b), a lower right inset], which has a lower packing density of equi-radial circles than the HCP structure, the value of N_j/N_b is 1/2. Experimentally, average values of N_j/N_b for creases form on the surface of hydrogel with varying thickness are found to have almost constant number of 0.58 irrespective of $\lambda_{c,max}$, which appears in the skeletonized images as the mixture of hexagonal cells (ideal) and square, pentagonal or open hexagonal cells (nonideal). When nucleated creases become long ($\sim\lambda_{c,max}$) and dense enough to encounter adjacent creases, the directions of growing creases are shifted away from the adjacent creases as further growth over the existing ones is restricted by the significant amount of energy barrier. In addition, creases are also found to shift laterally, break into two parts, or bend as they grow,[18] and the packing density of creases increases as the result of such rearrangement. However, achieving a higher packing density of creases—ultimately the HCP structure—requires a larger number of adjacent creases to move simultaneously, which imposes a greater amount of energy barrier to overcome for the rearrangement. Therefore, the rearrangement is eventually trapped in the metastable state, and N_j/N_b becomes less than 2/3. Based on almost constant value of N_j/N_b, we infer that the maximum level of rearrangement, thus packing density of creases, is almost unaffected by $\lambda_{c,max}$ but depends on the equilibrium level of swelling and/or the elasticity of the hydrogel, both of which are identical for the current system.

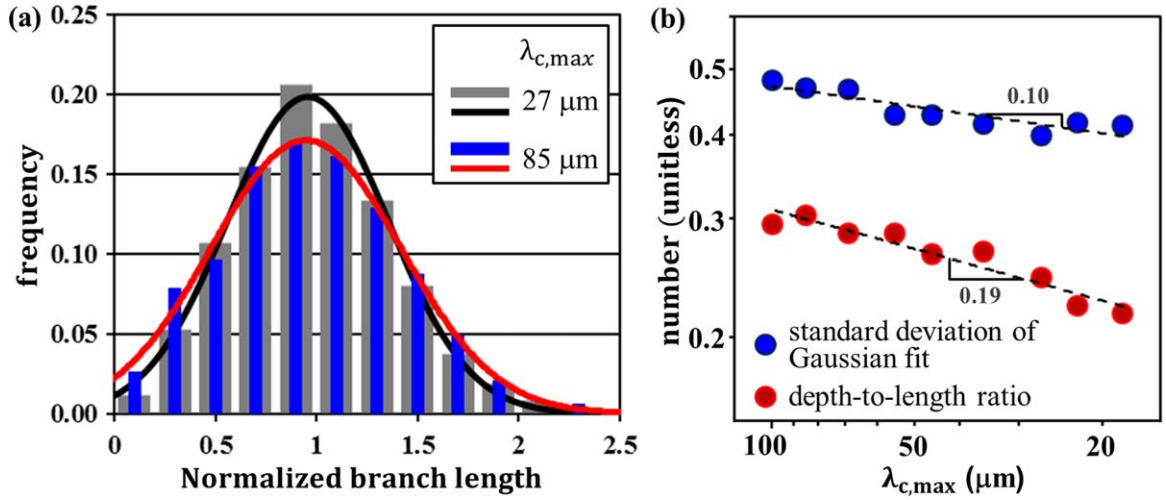

Figure 4. Nonself-similar features of crease patterns for varying $\lambda_{c,max}$. (a) Histograms of normalized contour length of branch at $\lambda_{c,max}$ of 85 μm (blue bars) and 27 μm (grey bars). The distributions are fitted with a Gaussian curve, whose standard deviation is measured at each $\lambda_{c,max}$. (b) A plot of the standard deviation of the Gaussian fit for the distribution of branch lengths (blue circles) and the depth-to-length ratio of creases (red circles) against $\lambda_{c,max}$. Both numbers, i.e., the standard deviations and the depth-to-length ratios, show a positive correlation with $\lambda_{c,max}$. [Color figure can be viewed in the online issue, which is available at wileyonlinelibrary.com.]

Next, we measure the ratio of contour length to Euclidean length of branches, l_c/l_E, to compare the curviness of creases at different $\lambda_{c,max}$. Figure 3(c) shows the average values of l_c/l_E at each $\lambda_{c,max}$. As in the previous case of N_j/N_b, the average of l_c/l_E is found to have almost constant value of 1.08. Here, we define curviness as the inplane bending of highly compressed regions along creases. Therefore, curviness of creases generates elastic deformation energy of bending. At the same time, however, it increases contour length of creases, and therefore, releases a larger amount of equi-biaxial compressive stress stored in the surface-attached hydrogel. In this regard, curviness of creases is determined by the balance between bending energy and additional release of compressive energy, which can be scaled as

$$E\frac{\Delta^3}{R^2}(at)l_c \sim E(l_c-l_E)(at)^2 \quad (1)$$

where E is the effective elastic modulus, Δ is the characteristic width of crease perpendicular to the growth direction of crease, R is the inplane radius of curvature of crease, at is the depth of crease—product of the hydrogel thickness t and the proportionality constant a—and l_c and l_E are contour and Euclidean lengths of branch, respectively. Rearranging the eq. 1 gives

$$\left(1-\left(\frac{l_c}{l_E}\right)^{-1}\right) \sim \frac{\Delta^3}{atR^2} \quad (2)$$

where $t \sim \lambda_{c,max}$ and $l_c/l_{E_{avg}} \sim 1.08$ irrespective of $\lambda_{c,max}$. Because R is a linear function of l_c at constant value of l_c/l_E and also $l_E \sim \lambda_{c,max}$, R becomes linearly proportional to $\lambda_{c,max}$. Therefore, we find that the characteristic width of crease Δ is linearly proportional to $\lambda_{c,max}$.

Nonself-Similar Features of Crease Patterns Formed on the Hydrogel with a Gradient in Thickness

While the two ratios, N_j/N_b and l_c/l_E, are found to have almost constant values for the range of $\lambda_{c,max}$ studied here, we find that several morphological features of crease patterns have a nonlinear dependence on $\lambda_{c,max}$.

We first examine the distribution of contour length of branch at each $\lambda_{c,max}$ (Figure 4). Figure 4(a) shows the representative histograms of normalized contour length of branch at $\lambda_{c,max}$ of 85 and 27 μm along with the least-square fits with a Gaussian distribution. The standard deviation of the Gaussian fit for each $\lambda_{c,max}$ is shown in Figure 4(b). Although the values are scattered to some extent, there is a tendency for the Gaussian fit to narrower as $\lambda_{c,max}$ becomes smaller, which is indicated by the positive value of the exponent of power law fit of 0.10. Compared to the exponents of power law fits for the plots of N_j/N_b and l_c/l_E against $\lambda_{c,max}$ (Figure 3), which are on the order of 10^{-3}, the value of 0.10 is of significance. We suppose that such variation in the distribution of branch length at each $\lambda_{c,max}$ is resulted from the thickness dependent variation in the kinetics of swelling and creasing of hydrogel. For example, it has been reported that the time required for the hydrogel to reach the equilibrium swelling by diffusion is determined by the thickness of hydrogel, which as well affects the kinetics of crease nucleation and the velocity of growing creases.[18] In particular, we infer that the nucleation of creases for the thinner hydrogel, or the hydrogel with smaller $\lambda_{c,max}$, is more homogeneous than that for the thicker hydrogel, which results in narrower distribution of branch length.

Furthermore, the morphological feature of crease pattern in the out-of-plane direction is also examined by comparing the depth of creases at each $\lambda_{c,max}$. We measure the average depth of crease at each $\lambda_{c,max}$ by dividing the surface area folded within creases, which were not deposited by PLL-FITC and, therefore, have a black color in Figure 2(a), by the total length of creases. Figure 4(b) shows the plot of the depth-to-length ratio, which is the only dimensional characteristic of creases in the out-of-plane direction, against $\lambda_{c,max}$. The plot shows the tendency for the

depth-to-length ratio to decrease as $\lambda_{c,max}$ becomes smaller with the exponent of power law fit of 0.19. We infer that such nonself-similar characteristic of crease, indicated by the $\lambda_{c,max}$ dependency of the depth-to-length ratio, is originated from the effect of surface tension.[19,20] It has been reported that the onset strain of crease formation (ε_0), beyond which nucleated creases start to grow, is found to be inversely proportional to the thickness of hydrogel due to the effect of surface tension.[18] Therefore, a thinner hydrogel experiences a higher ε_0, resulting in the formation of shallower creases at a given compressive strain, and therefore, the smaller value of the depth-to-length ratio of creases. However, the elastocapillary length scale h_{ec}, below which the effect of surface tension is comparable to or overwhelming the elasticity of hydrogel, i.e., the compressive stress, for the current water/hydrogel system is on the order of

$$h_{ec} = \frac{\gamma}{G} = 0.1 - 1 \ \mu m \quad (3)$$

where γ is the interfacial tension between water and hydrogel and G is the shear modulus of hydrogel, estimated to be on the order of 10^{-1} to 10^{0} dyne/cm[21] and 1 kPa, respectively. Therefore, considering the thickness of hydrogel studied here (from 20 to 120 μm), which is much greater than the elasto-capillary length scale, we infer that the effect of surface tension is only the minor contribution to the $\lambda_{c,max}$ dependency of the depth-to-length ratio of creases.

Instead, we suspect that such dependency, i.e. nonself-similar characteristic, is mainly originated from the formation of the polyelectrolyte complex between polycation (PLL-FITC) and negatively charged hydrogel, which occurs during the deposition of PLL-FITC on the surface of hydrogel. The complex formation neutralizes the fixed negative charges of hydrogel, and therefore, reduces the osmotic pressure responsible for the swelling of hydrogel.[8] By using laser scanning confocal microscopy, we measure the depth into which PLL-FITC forms polyelectrolyte complex with hydrogel, which is approximately 5 μm independent of the lateral position, and therefore, the thickness of hydrogel. The effect of complex formation on the reduction of swelling of hydrogel becomes more significant at the thinner part of the hydrogel, which has a higher fraction of its negative charges being neutralized by the complex formation. Therefore, the thinner part of hydrogel experiences a greater level of unfolding of creases during the PLL-FITC deposition step, which results in the smaller value of the depth-to-length ratio of creases.

CONCLUSIONS

The morphology of crease patterns formed on the surface-attached hydrogel with a gradient in thickness has been analyzed using the fluorescent microscopy and various image analysis techniques. To visualize the morphology of creases, the surface of hydrogel at the creased state is labeled with the fluorescent polymer. At the deswelled state, the surface areas once folded within creases, and therefore, not labeled by the fluorescent polymer are exposed, which enables us to visualize the surface morphology of crease patterns using the fluorescent microscopy. Using image analysis techniques, we analyze several morphological characteristics of crease pattern. For examples, at each $\lambda_{c,max}$, the ratio of the number of junction to that of branch is measured to infer packing geometry of crease patterns, and the ratio of contour length to Euclidean length of branch is analyzed to characterize the curviness of creases, where both features show morphological self-similarity, i.e., no dependence on $\lambda_{c,max}$. However, the distribution of contour length of crease and the depth-to-length ratio of crease are found to have a weak dependence on $\lambda_{c,max}$, presumably due to the $\lambda_{c,max}$ dependency of the kinetics of swelling and creasing of hydrogel, the effect of surface tension, and the reduction in swelling of hydrogel during the PLL-FITC deposition step.

ACKNOWLEDGMENTS

This work was supported by the Sogang University Research Grant of 201210045.01.

REFERENCES

1. Cerda, E.; Ravi-Chandar, K.; Mahadevan, L. *Nature* **2002**, *419*, 579.
2. Trujillo, V.; Kim, J.; Hayward, R. C. *Soft Matter* **2008**, *4*, 564.
3. Brau, F.; Vandeparre, H.; Sabbah, A.; Poulard, C.; Boudaoud, A.; Damman, P. *Nat. Phys.* **2011**, *7*, 56.
4. Cerda, E.; Mahadevan, L. *Phys. Rev. Lett.* **2003**, *90*, 074302.
5. Cai, S. Q.; Chen, D. Y.; Suo, Z. G.; Hayward, R. C. *Soft Matter* **2012**, *8*, 1301.
6. Chan, E. P.; Smith, E. J.; Hayward, R. C.; Crosby, A. J. *Adv. Mater.* **2008**, *20*, 711.
7. Jeong, H. E.; Kwak, M. K.; Suh, K. Y. *Langmuir* **2010**, *26*, 2223.
8. Kim, J.; Yoon, J.; Hayward, R. C. *Nat. Mater.* **2010**, *9*, 159.
9. Lin, P. C.; Vajpayee, S.; Jagota, A.; Hui, C. Y.; Yang, S. *Soft Matter* **2008**, *4*, 1830.
10. Yang, S.; Khare, K.; Lin, P. C. *Adv. Funct. Mater.* **2010**, *20*, 2550.
11. Yoon, J.; Bian, P.; Kim, J.; McCarthy, T. J.; Hayward, R. C. *Angew. Chem. Int. Ed.* **2012**, *51*, 7146.
12. Chan, E. P.; Crosby, A. J. *Adv. Mater.* **2006**, *18*, 3238.
13. Nolte, A. J.; Rubner, M. F.; Cohen, R. E. *Macromolecules* **2005**, *38*, 5367.
14. Stafford, C. M.; Harrison, C.; Beers, K. L.; Karim, A.; Amis, E. J.; Vanlandingham, M. R.; Kim, H. C.; Volksen, W.; Miller, R. D.; Simonyi, E. E. *Nat. Mater.* **2004**, *3*, 545.
15. Stafford, C. M.; Vogt, B. D.; Harrison, C.; Julthongpiput, D.; Huang, R. *Macromolecules* **2006**, *39*, 5095.
16. Saha, K.; Kim, J.; Irwin, E.; Yoon, J.; Momin, F.; Trujillo, V.; Schaffer, D. V.; Healy, K. E.; Hayward, R. C. *Biophys. J.* **2010**, *99*, L94.
17. Li, B.; Cao, Y. P.; Feng, X. Q.; Gao, H. J. *Soft Matter* **2012**, *8*, 5728.
18. Yoon, J.; Kim, J.; Hayward, R. C. *Soft Matter* **2010**, *6*, 5807.
19. Kang, M. K.; Huang, R. *Soft Matter* **2010**, *6*, 5736.
20. Chen, D. Y.; Cai, S. Q.; Suo, Z. G.; Hayward, R. C. *Phys. Rev. Lett.* **2012**, *109*, 038001.
21. King, R. N.; Andrade, J. D.; Ma, S. M.; Gregonis, D. E.; Brostrom, L. R. *J. Colloid. Interf. Sci.* **1985**, *103*, 62.